Electronic Supplementary Material (ESI) for Energy & Environmental Science

Supplementary Information

Facile Colloidal Synthesis of Quinary $CuIn_{1-x}Ga_x(S_ySe_{1-y})_2$ (CIGSSe) Nanocrystal Inks with Tunable Band Gaps for Use in Low-Cost Photovoltaics

Shu-Hao Chang,[a] Ming-Yi Chiang,[a] Chien-Chih Chiang,[b] Fang-Wei Yuan,[a] Chia-Yu Chen,[a] Bo-Cheng Chiu,[a] Tzu-Lun Kao,[a] Chi-Huang Lai[c] and Hsing-Yu Tuan*[a]

a Department of Chemical Engineering, National Tsing Hua University, Hsinchu, Taiwan 30013, Republic of China.

b Green Energy & Environment Research Laboratories (GEL), Industrial Technology Research Institute (ITRI), Hsinchu, Taiwan 31040, Republic of China

c Department of Materials Science and Engineering, National Tsing Hua University, Hsinchu, Taiwan 30013, Republic of China

Corresponding Author

*Hsing-Yu Tuan, Phone: (886)3-5723661; Fax: (886)3-571-5408
E-mail: hytuan@che.nthu.edu.tw

Experimental Methods

Chemicals:

All reagents were used as received. Copper(I) chloride (CuCl; 99.995+%), indium(III) chloride ($InCl_3$; anyhydrous 99.99%), gallium(III) chloride ($GaCl_3$;99.9999%), elemental sulfur (99.98%), elemental selenium (99.99%), hexane, toluene, oleylamine (70%) and ethanol (ACS reagent grade, >99.5%) from Aldrich Chemical Co.

Synthesis of $CuIn_{1-x}Ga_x(S_ySe_{1-y})_2$ (CIGSSe) nanocrystals

The precursors were carefully weighted using a balance with an uncertainty of ± 0.1 mg (Mettler Toledo AL204). Reactions were performed using a Schlenk manifold under a purified argon atmosphere. In a typical synthesis, 0.5 mmol of CuCl (0.0495 g), 0.5 mmol total of $InCl_3$ (0.0000 to 0.1106 g), $GaCl_3$ (0.0000 to 0.0880 g) and 1 mmol total of elemental Se (0.0000 to 0.0790 g) and elemental S (0.0000 to 0.0320g), 12 ml oleylamine, and a glass-coated stir bar were loaded into a 50-mL three-neck flask. The flask was placed on a magnetic hot plate (Thermo Scientific). The 50-mL flask was then attached to the Schlenk line. The temperature was monitored and controlled using a thermocouple and a PID temperature controller through the third neck of the flask. The flask was purged off air and water by argon and bubbling at 130 °C for 1 h in a vigorously stirring. Next, the system was slowly heated to 265 °C with a 2.3 °C/min raising rate and kept at this temperature for 1.5 h at vigorous stirring. After reaction, the flask was quenched in a cold water bath to quickly bring the temperature down. The CIGSSe nanocrystal/oleylamine solution was transferred to a 50-mL centrifuge tube. 10 ml of hexane and 15 ml of ethanol were added to the nanocrystal solution and centrifuged at 8000 rpm for 10 min. The centrifuge purification procedure was repeated several times until the supernatant was clear. The nanocrystals were in the precipitate and collected, whereas the supernatant containing byproducts and unreacted precursor was discarded. The nanocrystals were redispersed in hexane or toluene for further characterization.

Gram-scale synthesis of $CuIn_{0.5}Ga_{0.5}(S_{0.5}Se_{0.5})_2$ nanocrystals

For gram-scale synthesis, a 500 mL three-neck flas was used as a reactor. The reaction was carried out in the presence of 5 mmol of CuCl (0.495 g), 2.5 mmol of $InCl_3$ (0.553 g), 2.5 mmol of $GaCl_3$ (0.44 g), 5 mmol of elemental Se (0.395 g), 5 mmol of elemental S (0.161 g), and 120 ml oleylamine in the 500-mL three-neck flask with a slow heating rate and holding the synthesis at 265 °C for 1.5 h. The purified procedure was same as the statement before.

CIGSSe-based thin film solar cell fabrication

The Mo coated soda lime glass substrates were fabricated by DC magnetron sputtering resulting in a 500 nm layer. The CIGSSe absorber layer made using $CuIn_{0.7}Ga_{0.3}(S_{0.5}Se_{0.5})_2$ nanocrystals as a absorber layer precursor was were spray-coated on the top of Mo substrates by airbrush (KUSING BD-130, 0.3mm), operated about 20 psig of head pressure. And then, the thin film subsequent

annealed in Ar and Se atmospheres at 450 °C and selenized in a graphite box at 550 °C with rapid heating. A 80 nm CdS layer was then deposited by a chemical bath deposition (CBD) technique. The CBD bath contains 183 ml of deionized H_2O, 25 ml of 0.015 M $CdSO_4$ solution, 12.5 of 1.5 M thiourea solution, and 31.25 ml of stock NH_4OH (Aldrich). Next, a thin 100 nm high resistivity ZnO film capped with a ~500 nm high conductivity Al doped ZnO (AZO) layer were deposited by RF magnetron sputtering. The ZnO film was sputtered in a mixture of 10 % O_2 in Ar at sputtering pressure of 10 mTorr with no intentional heating. The AZO layer was sputtered with neither O_2 nor intentional heating at sputtering pressure of 1 mTorr. After sputtering oxide layers, the final device was scribed into small area devices with colloidal silver paste as top contact (~0.15 cm^2 reduce the area of Ag electrode).

Characterization

Nanocrystals were characterized using various instruments, including transmission electron microscopy (TEM), X-ray diffraction (XRD), energy-dispersive X-ray spectroscopy (EDS), X-ray photoelectron spectroscopy (XPS), UV-vis-NIR absorbance spectrophotometer and cyclic voltammetry (CV).

TEM sample was prepared by dropping an aliquot of nanocrystals in hexane on a carbon-coated 200 mesh titanium or nickel TEM grids. TEM images were obtained on JEOL JEM-1200 or Hitachi H-7100 TEM at an accelerating voltage of 120 kV for low resolution imaging and on a Tecnai G^2 F20 X-Twin microscope at an accelerating voltage of 200 kV, respectively. The Tecnai G^2 F20 X-Twin microscope is equipped with an Oxford INCA EDS detector for EDS analysis. Powder X-ray diffraction (XRD) analysis was performed on a Rigaku Ultima IV X-ray diffractometer using a Cu Kα radiation source (λ = 1.54 Å). XRD data were collected for the powders of $CuIn_{1-x}Ga_x(S_ySe_{1-y})_2$ nanoparticles on a glass substrate by scanning for 12 h at a rate of 0.016 deg/s. X-ray photoelectron spectroscopy (XPS) analysis was performed on Kratos Axis Ultra DLD using 500 mm Rowland circle Al monochromator. For XPS sample preparation, the nanocrystals were drop-casting on a 0.5×0.5 cm wafer in an argon-filled glove box. UV-Vis-NIR absorbance spectra of nanocrystals dispersion in toluene were obtained by a Hitachi U-4100 UV-vis-NIR spectrophotometer at room temperature. FTIR Spectra were recorded by dispersing $CuIn_{0.5}Ga_{0.5}(S_{0.5}Se_{0.5})_2$ nanoparticles in hexane and placing a small drop of the solution on one of the KBr plates. Place the second KBr plate on top to get a nice even film. The KBr plates should be carefully cleaned after measurement to prevent contamination of other samples. Cyclic voltammetry (CV) were recorded on a multi-channel electrochemical analyzer (Bio-Logic-Science Instruments, VMP3), using glassy carbon as working electrode, 0.1 M tetrabutylammonium hexafluorophosphate ($TBAPF_6$) dissolved in acetonitrile was as the electrolyte, Ag/Ag^+ (Ag wire with 0.01 M $AgNO_3$ and 0.1 M $TBAPF_6$ in acetonitrile) as the reference electrode, and a platinum foil as a counter electrode. All nanocrystals samples were purified and dissolved in toluene. 1-2 mg nanocrystals deposited directly on glassy carbon electrode. The electrolyte solutions were thoroughly degassed with argon for 30 min; and the scan rate was set

at 40 mV/s.

PV response was measured using a Xenon Lamp solar simulator under simulated AM 1.5 illumination (Continuous Solar Simulator for PV Cells, Hong-ming Technology Co., Ltd.). External quantum efficiency (EQE) was collected by a EQE Measurement System (Continuous Solar Simulator for PV Cells, Hong-ming Technology Co., Ltd.).

Additional results

STEM-EDS mapping of $CuIn_{0.5}G_{0.5}(S_{0.5}Se_{0.5})_2$ nanocrystals

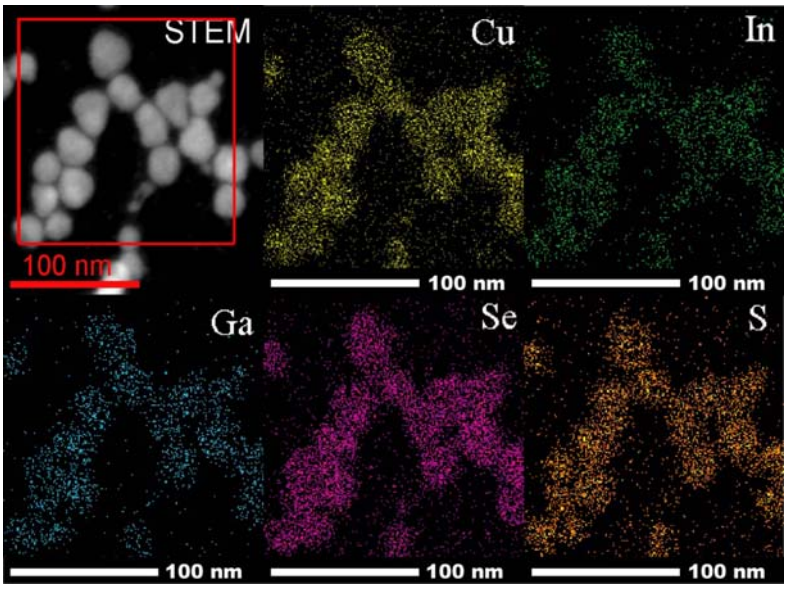

Fig. S1 Scanning transmission electron microscopy (STEM-EDS) mapping of $CuIn_{0.5}G_{0.5}(S_{0.5}Se_{0.5})_2$ nanocrystals confirms the five elements are equally distributed within the nanocrystals.

XPS spectra

XPS was used to investigate the chemical state of the $CuIn_{0.5}G_{0.5}(S_{0.5}Se_{0.5})_2$ nanoparticles. Fig. S2 shows XPS spectra of oleylamine-capped $CuIn_{0.5}G_{0.5}(S_{0.5}Se_{0.5})_2$ nanocrystals. The Cu2p, In3d, Ga2p, Se3d, S2p, Se3p regions were labeled. All binding energies have been corrected by referencing the C 1s (284.6 eV). The Cu 2p peak is split into Cu $2p_{3/2}$ (932.4eV) and Cu $2p_{1/2}$ (952.3eV) peaks with a peak separation of 19.9 eV (Fig. S2a), in agreement with those reported in the literature for the CIS nanocrystals,[1] suggesting that the copper valence state in the $CuIn_{0.5}G_{0.5}(S_{0.5}Se_{0.5})_2$ nanocrystals is +1. The Indium 3d peaks locate at 445.0 and 452.5 eV with a peak separation of 7.5 eV in Fig. S2b, consistent with a valence of +3.[2] Fig. S2c indicates that the gallium $2p_{3/2}$, $2p_{1/2}$ peaks locate at 1118.0 and 1145.0 eV, and the peak separation is 27 eV, consistent with the reported values.[3] Fig. S2d shows the selenium $3d_{5/2}$ peak located at 53.9 eV, a little smaller to Se $3d_{5/2}$ of $CuIn(S_{0.5}Se_{0.5})_2$ (54.1 eV),[4] confirming its state -2. To determine the peak energy of the S 2p and Se 3p peaks, computational

peak separation was made. The S 2p peak is split by spin-orbit coupling into a doublet. Fig. S2e shows the S 2p and Se 3p core levels fitted to doublets by a mixed Gaussian and Lorentzian profile. Each S 2p consists of a spin-orbit-split doublet with the S $2p_{3/2}$ (161.7 eV) and S $2p_{1/2}$ (162.8eV), with a peak energy split by 1.1 eV and an area ratio close to 0.5. The ratio is in agreement with the literature values.[5] The two peaks of S 2p in Fig. S2e were consistent with a valence of -2. The Se 3p peak is split into two components (spin-orbit coupling) at 160.5 and 166.3 eV with a peak separation of 5.8 eV.

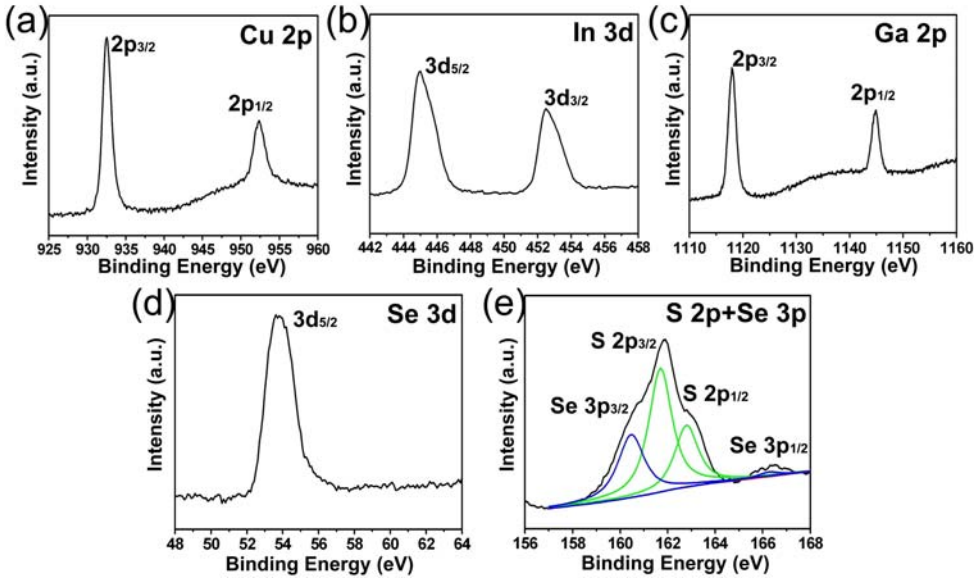

Fig. S2 XPS spectra of $CuIn_{0.5}G_{0.5}(S_{0.5}Se_{0.5})_2$ nanocrystals.

Characterization of $CuIn_{0.5}G_{0.5}(S_{0.5}Se_{0.5})_2$ nanocrystals synthesized from gram-scale synthesis

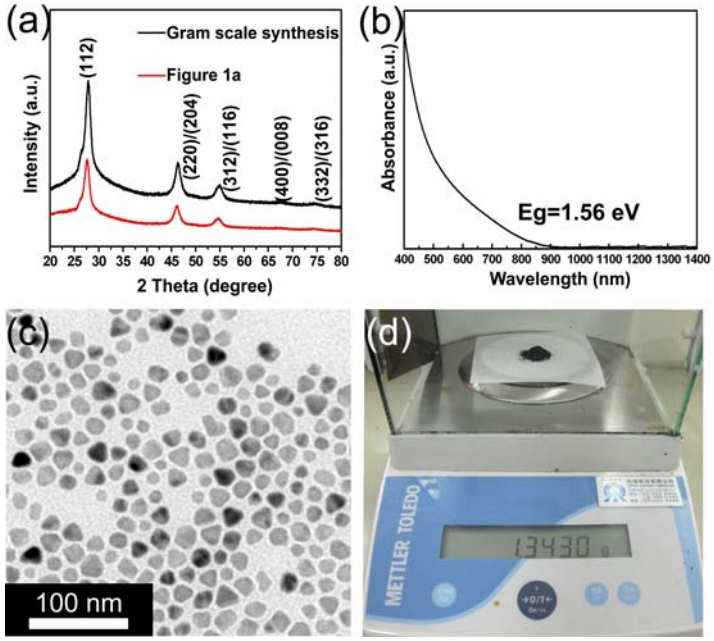

Fig. S3 (a) XRD patterns of $CuIn_{0.5}G_{0.5}(S_{0.5}Se_{0.5})_2$ nanocrystals from 1.343 g $CuIn_{0.5}G_{0.5}(S_{0.5}Se_{0.5})_2$ nanocrystals, showing the same diffraction peaks with the normal scale (Fig. 1a) (b) UV-vis-NIR absorption spectra of $CuIn_{0.5}G_{0.5}(S_{0.5}Se_{0.5})_2$ with a optical band gap of 1.56 eV (c) TEM images of $CuIn_{0.5}G_{0.5}(S_{0.5}Se_{0.5})_2$ nanocrystals (d) Digital pictures of 1.343g $CuIn_{0.5}G_{0.5}(S_{0.5}Se_{0.5})_2$ nanocrystal. Samples were collected after repeated purification procedures.

Lattice parameter analysis

For many reports, the Cu–In–Se, Cu-Ga-S, and Cu–In–Ga–Se present a chalcopyrite structure (tetragonal crystal system) belonging to space group $I\bar{4}2d$.[6-8] Chalcopyrite can be considered as a superstructure of two zinc blende structures. The chalcopyrite (tetragonal) lattice is characterized by lattice constants **a** and **c**. A corresponding formula in tetragonal crystal system is as shown in below.

$$\frac{1}{d^2} = \frac{h^2 + k^2}{a^2} + \frac{l^2}{c^2} \qquad \text{(S1)}$$

where d is the d-spacing(interplanar distance), a and c represent the lengths of the unit cell edges; h, k, and l are called crystallographic or Miller indices.

The formula illustrates dependence of the d-spacing on the Miller indices of the family and the lengths of the three-unit cell edges. According to the Braggs' law, the diffraction angle diffraction angle (θ_{hkl}) of a reflection from a series of lattice planes (hkl) can be determined from the d-spacing and the wavelength as follow equation:

$$\sin\theta_{hkl} = \frac{\lambda}{2d_{hkl}} \qquad \text{(S2)}$$

The lattice parameters a and c can be easily calculated from the formulas. The lattice parameters (a and c) versus composition plotted in Fig. S4.

In this system, the lattice constants are varied with the composition and showing that Vegard's law holds well for the lattice constant. According to Vegard's law, the lattice pentanary alloyed $CuIn_{1-x}Ga_x(S_ySe_{1-y})_2$ nanocrystals can be express as :

$$a_{CuIn_{1-x}Ga_x(S_ySe_{1-y})_2} = xya_{CuGaS_2} + x(1-y)a_{CuGaSe_2} + (1-x)ya_{CuInS_2} + (1-x)(1-y)a_{CuInSe_2} \qquad \text{(S3)}$$

$$c_{CuIn_{1-x}Ga_x(S_ySe_{1-y})_2} = xyc_{CuGaS_2} + x(1-y)c_{CuGaSe_2} + (1-x)yc_{CuInS_2} + (1-x)(1-y)c_{CuInSe_2} \qquad \text{(S4)}$$

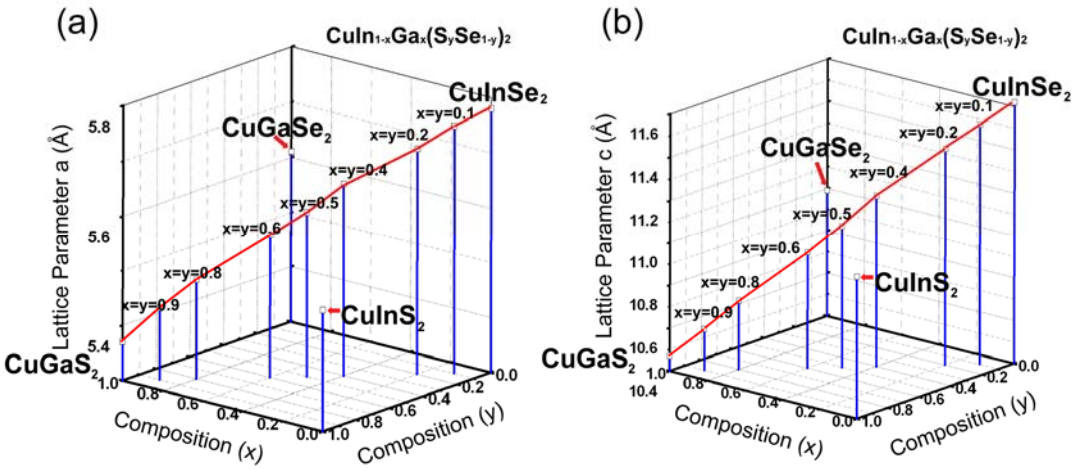

Fig. S4 Lattice constants vs. composition for $CuIn_{1-x}Ga_x(S_ySe_{1-y})_2$ nanocrystals, which show good agreement with Vegard's law(red lines) and further confirm the formation of a complete $CuIn_{1-x}Ga_x(S_ySe_{1-y})_2$ alloy.

Table S1. Lattice parameters and unit-cell volume for $CuIn_{1-x}Ga_x(S_ySe_{1-y})_2$

$CuIn_{1-x}Ga_x(S_ySe_{1-y})_2$	Experimental		Vegard's law	
	a (Å)	c (Å)	a (Å)	c (Å)
x=y=0.1	5.75	11.52	5.74	11.51
x=y=0.2	5.71	11.41	5.70	11.40
x=y=0.4	5.65	11.20	5.61	11.18
x=y=0.5	5.60	11.06	5.57	11.06
x=y=0.6	5.56	10.94	5.52	10.95
x=y=0.8	5.48	10.72	5.44	10.71
x=y=0.9	5.41	10.51	5.39	10.59
x=0.3, y=0.5	5.65	11.15	5.60	11.19
x=0.7, y=0.5	5.51	10.87	5.53	10.93

TEM and HRTEM images of $CuIn_{1-x}Ga_x(S_ySe_{1-y})_2$ nanocrystals

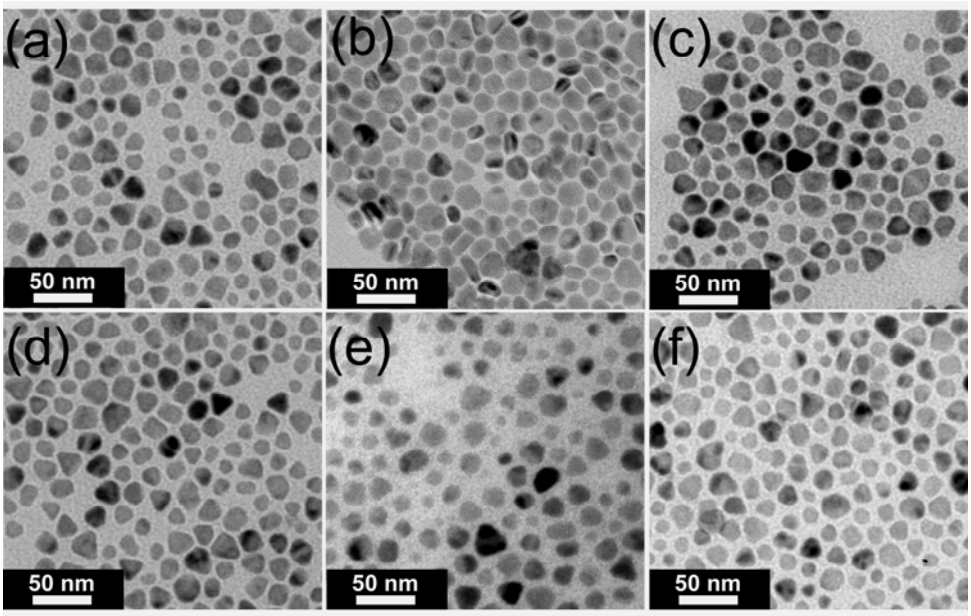

Fig. S5 TEM images of $CuIn_{1-x}Ga_x(S_ySe_{1-y})_2$ nanocrystals with (a) x=y=0.1, (b) x=y=0.2, (c) x=y=0.4, (d) x=y=0.6, (e) x=y=0.8, and (f) x=y=0.9

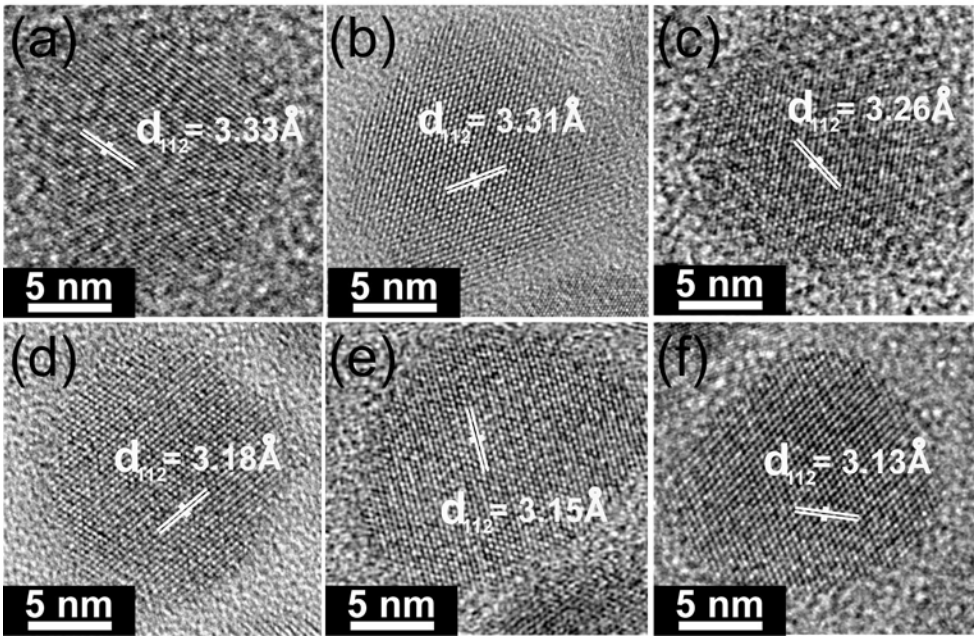

Fig. S6 HRTEM images of $CuIn_{1-x}Ga_x(S_ySe_{1-y})_2$ nanocrystals with (a) x=y=0.1, (b) x=y=0.2, (c) x=y=0.4, (d) x=y=0.6, (e) x=y=0.8, and (f) x=y=0.9. The lattice spacings of (112) in each nanocrystal increase gradually.

Determination of optical band gap from UV-Vis-Near spectra:

The direct allowed optical band gap Eg can be determined with the relation:[9]

$$\alpha h\nu = D(h\nu - E_g)^n \tag{S5}$$

where D is a constant, hν is the photon energy, and E_g is the optical band gap.

For a direct transition, n=1/2. By extrapolating the linear part of the plot to $(\alpha h\nu)^2 = 0$, values of the direct band gap E_g for each composition x were determined.

The experimental values of $(\alpha h\nu)^2$ against hν is plotted in Fig. S7.

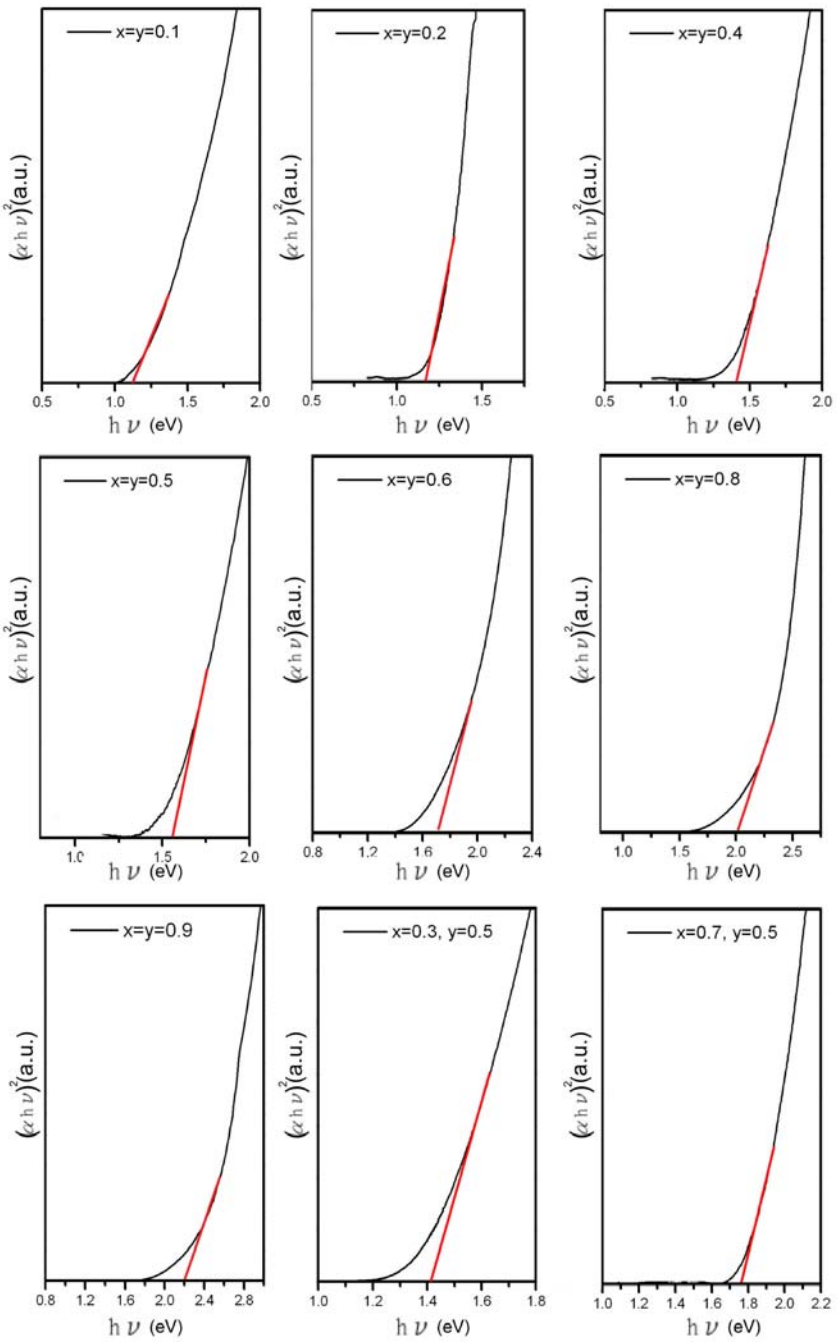

Fig. S7 Plot of $(\alpha h\nu)^2$ vs. (hν) for the $CuIn_{1-x}Ga_x(S_ySe_{1-y})_2$ system

Band gap profile approximation of $CuIn_{1-x}Ga_x(S_ySe_{1-y})_2$

Band gap energy of $CuIn_{1-x}Ga_x(S_ySe_{1-y})_2$ depending on $0 \leqq x \leqq 1$ and on $0 \leqq y \leqq 1$ may be approximated from the binary models which yield an expression for Eg of the $CuIn_{1-x}Ga_x(S_ySe_{1-y})_2$ alloy:

$$E_g^{CIGSSe}(x,y) = (1-y)[(1-x)E_g^{CISSe}(y) + x\,E_g^{CGSSe}(y) - b^{CIGSe}x(1-x)] + y[(1-x)E_g^{CISSe}(y) + xE_g^{CGSSe}(y) - b^{CIGS}x(1-x)] \quad (1)$$

$$E_g^{CISSe}(y) = yE_g^{CuInS_2} + (1-y)E_g^{CuInSe_2} - b^{CISSe}y(1-y) \quad (S6)$$

$$E_g^{CGSSe}(y) = yE_g^{CuGaS_2} + (1-y)E_g^{CuGaSe_2} - b^{CGSSe}y(1-y) \quad (S7)$$

$$E_g^{CIGS}(x) = xE_g^{CuGaS_2} + (1-x)E_g^{CuInS_2} - b^{CIGS}x(1-x) \quad (S8)$$

$$E_g^{CIGSe}(x) = xE_g^{CuGaSe_2} + (1-x)E_g^{CuInSe_2} - b^{CIGSe}x(1-x) \quad (S9)$$

Applying the corresponding band gap values for $CuInS_2$,[4] $CuInSe_2$ (Fig. 11a), $CuGaS_2$ (Fig. 11b), $CuGaSe_2$[10] (Table S2) and the optical bowing constants of CISSe,[4] CGSSe,[11] CIGS,[11] CIGSe[12] (Table S3), the equation can be simplified to the following expression:

$$E_g^{CIGSSe}(x,y) = (0.98 + 0.167x^2 + 0.17y^2 + 0.023x^2y - 0.17xy^2 + 0.397xy + 0.31y + 0.523x)\ eV \quad (2)$$

This equation was typed into Matlab and the result is shown in Fig. 4.

Table S2. Band gap energies of ternary chalcopyrites

$CuIn_{1-x}Ga_x(S_ySe_{1-y})_2$ alloy	Eg (eV)
x=0, y=0 : $CuInSe_2$	0.98
x=0, y=1 : $CuInS_2$	1.46
x=1, y=0 : $CuGaSe_2$	1.67
x=1, y=1 : $CuGaS_2$	2.4

Table S3. Optical bowing constants b for the quaternary chalcopyrites

$CuIn_{1-x}Ga_x(S_ySe_{1-y})_2$ alloy	b (eV)
x=0, $0 \leqq y \leqq 1$: $CuIn(S_ySe_{1-y})_2$ (CISSe)	0.17
x=1, $0 \leqq y \leqq 1$: $CuGa(S_ySe_{1-y})_2$ (CGSSe)	0
$0 \leqq x \leqq 1$, y=1 : $Cu(In_{1-x}Ga_x)S_2$ (CIGS)	0.19
$0 \leqq x \leqq 1$, y=0 : $Cu(In_{1-x}Ga_x)Se_2$ (CIGSe)	0.167

Cyclic voltammetry analysis:

Cyclic voltammetry (CV) is a dynamic electrochemical method to measure the band-edge positions of nanomaterials.[13] From CV spectra, the band-edge positions (i.e., the highest occupied molecular orbital (HOMO) and lowest unoccupied molecular orbital (LUMO) energy position) can be determined. Oxidation potential was correlated directly with the ionization potential(I_p) and the reduction potential with the electron affinity(E_a), the band edge positions of electroactive materials can be calculated.[14] The HOMO and LUMO energy levels can be derived from the onset oxidation potential (E_{ox}) and onset reduction potential (E_{red}), respectively, according to equation below:[13]

$$E_{HOMO}=-I_p=-(E_{ox}+4.71)\ eV \quad (S10)$$

$$E_{LUMO}=-E_a=-(E_{red}+4.71)\ eV \quad (S11)$$

where the onset of the potential values are relative to a Ag/Ag^+ reference electrode. The value of 4.71 represents the difference between the vacuum level potential of the normal hydrogen electrode (NHE) and the potential of the Ag/AgCl electrode versus NHE. We started from zero and the scanning voltage ranges was from -2.5 to 2.5 V. Fig. S8 outlines the onset potentials for the oxidation and reduction of our nanocrystals.

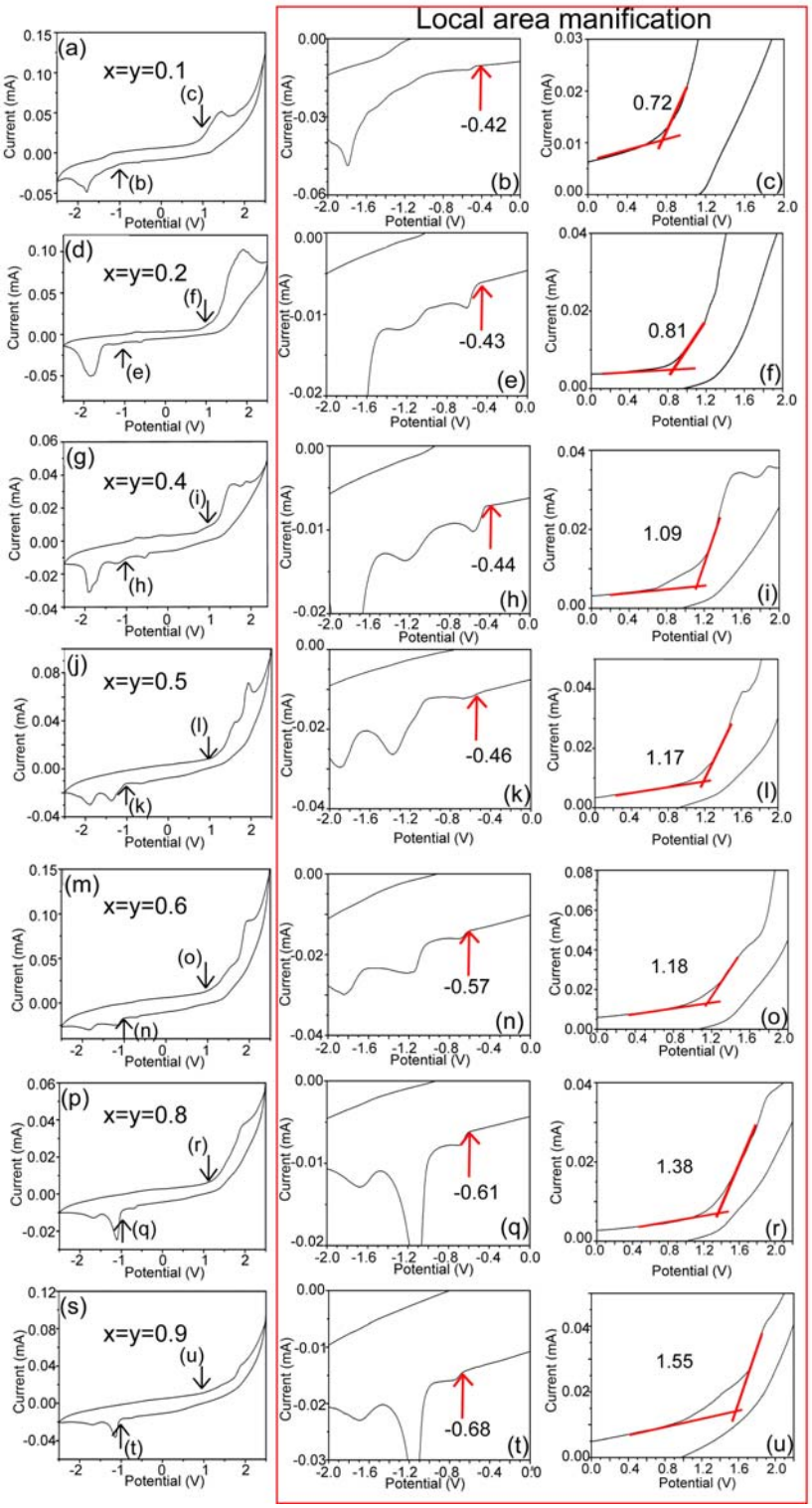

Fig. S8 CV analysis of $CuIn_{1-x}Ga_x(S_ySe_{1-y})_2$ nanocrystals. The black arrow direction is magnified area.

Table S4. Composition, Band Gap Energies of $CuIn_{1-x}Ga_x(S_ySe_{1-y})_2$ Nanocrystals determined by absorption spectra, CV, and Eq. (2)

Target compound $CuIn_{1-x}Ga_x(S_ySe_{1-y})_2$	Precursor composition (Cu/In/Ga/S/Se atom ratio %)	Composition measured by EDS (Cu/In/Ga/S/Se atom ratio %)	Eg (eV) determined by absorption spectra	Eg (eV) determined by CV	Eg (eV) determined by Eq. (2)
$CuIn_{0.9}Ga_{0.1}(S_{0.1}Se_{0.9})_2$	25 : 22.5 : 2.5 : 5 : 45	24.11 : 22.04 : 2.84 : 5.69 : 45.32	1.08	1.14	1.07
	(1 : 0.9 : 0.1 : 0.2 : 1.8)	(0.97 : 0.88 : 0.11 : 0.22 : 1.82)			
$CuIn_{0.8}Ga_{0.2}(S_{0.2}Se_{0.8})_2$	25 : 20 : 5 : 10 : 40	24.5 : 19.64 : 5.73 : 10.21 : 39.91	1.17	1.24	1.17
	(1 : 0.8 : 0.2 : 0.4 : 1.6)	(0.98 : 0.79 : 0.23 : 0.4 : 1.6)			
$CuIn_{0.6}Ga_{0.4}(S_{0.4}Se_{0.6})_2$	25 : 15 : 10 : 20 : 30	26.79 : 15.01 : 9.89 : 17.85 : 30.46	1.42	1.53	1.42
	(1 : 0.6 : 0.4 : 0.8 : 1.2)	(1.07 : 0.6 : 0.4 : 0.71 : 1.22)			
$CuIn_{0.5}Ga_{0.5}(S_{0.5}Se_{0.5})_2$	25 : 12.5 : 12.5 : 25 : 25	25.12 : 12.44 : 12.42 : 24.86 : 25.16	1.56	1.63	1.56
	(1 : 0.5 : 0.5 : 1.0 : 1.0)	(1 : 0.5 : 0.5 : 0.99 : 1.01)			
$CuIn_{0.4}Ga_{0.6}(S_{0.6}Se_{0.4})_2$	25 : 10 : 15 : 30 : 20	24.08 : 9.32 : 15 : 30.85 : 20.75	1.71	1.75	1.71
	(1 : 0.4 : 0.6 : 1.2 : 0.8)	(0.96 : 0.37 : 0.6 : 1.23 : 0.83)			
$CuIn_{0.2}Ga_{0.8}(S_{0.8}Se_{0.2})_2$	25 : 5 : 20 : 40 : 10	25.45 : 4.3 : 20.92 : 37.92 : 11.41	2.01	1.99	2.04
	(1 : 0.2 : 0.8 : 1.6 : 0.4)	(1.01 : 0.17 : 0.84 : 1.52 : 0.46)			
$CuIn_{0.1}Ga_{0.9}(S_{0.9}Se_{0.1})_2$	25 : 2.5 : 22.5 : 45 : 5	24.18 : 3.11 : 22.43 : 43.44 : 6.84	2.20	2.23	2.22
	(1 : 0.1 : 0.9 : 1.8 : 0.2)	(0.97 : 0.12 : 0.9 : 1.74 : 0.27)			

Characterization of $CuIn_{1-x}Ga_x(S_ySe_{1-y})_2$ nanocrystals with $x \neq y$

Synthesis $CuIn_{1-x}Ga_x(S_ySe_{1-y})_2$ nanocrystals with $x \neq y$ were also demonstrated by the developed method. Taking $CuIn_{0.7}Ga_{0.3}(S_{0.5}Se_{0.5})_2$ and $CuIn_{0.7}Ga_{0.3}(S_{0.5}Se_{0.5})_2$. as two representative examples as shown in Fig. S9 and Fig. S10.

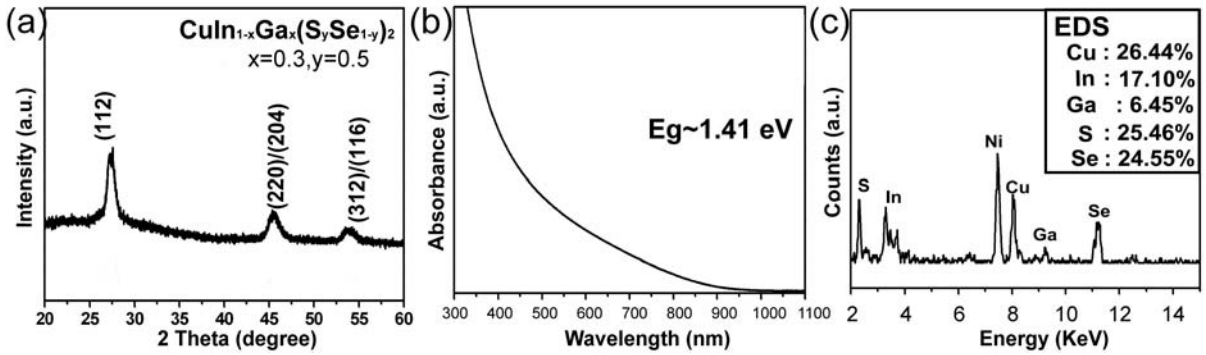

Fig. S9 (a) XRD patterns (b) UV-Vis-Near IR absorption spectra (c) EDS data of $CuIn_{0.7}Ga_{0.3}(S_{0.5}Se_{0.5})_2$ nanocrystals.

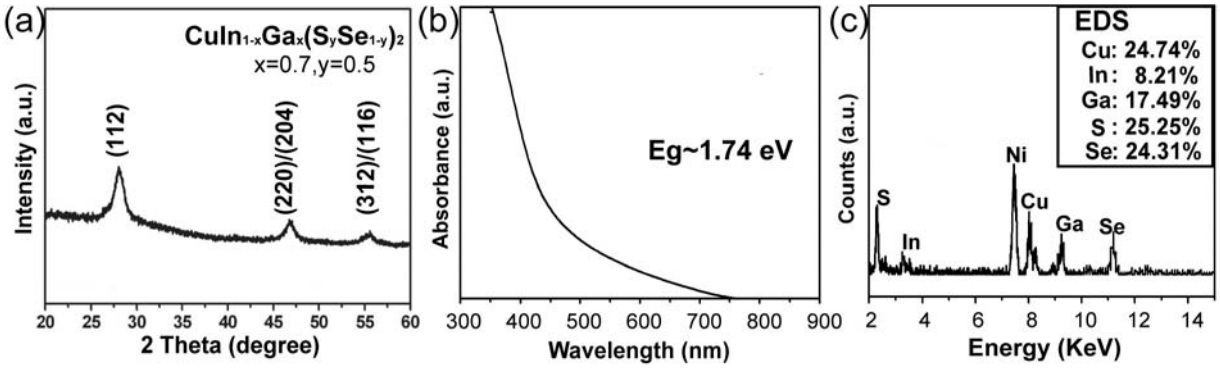

Fig. S10 (a) XRD patterns (b) UV-Vis-Near IR absorption spectra (c) EDS data of $CuIn_{0.3}Ga_{0.7}(S_{0.5}Se_{0.5})_2$ nanocrystals.

Absorption spectra of $CuIn_{1-x}Ga_x(S_ySe_{1-y})_2$ nanocrystals with x=0,y=1($CuInSe_2$), and x=1, y=0 ($CuGaS_2$)

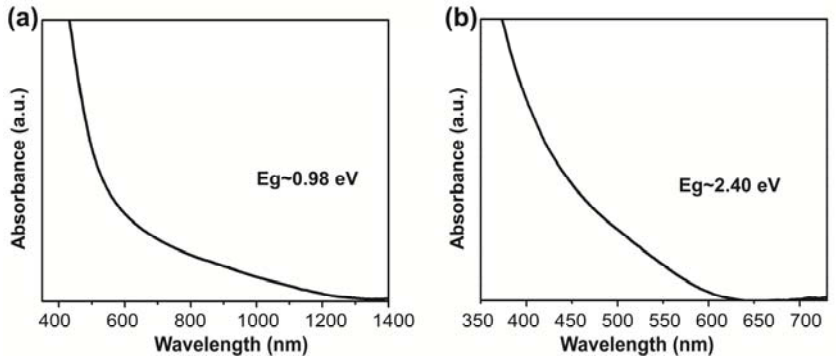

Fig. S11 UV-Vis-NIR absorption spectra of (a) $CuInSe_2$ (b) $CuGaS_2$ nanocrystals.

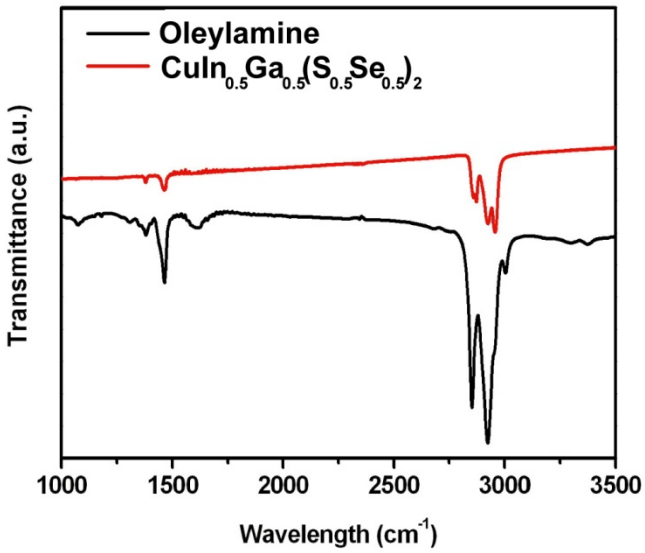

Fig. S12. FTIR pattern of $CuIn_{0.5}Ga_{0.5}(S_{0.5}Se_{0.5})_2$ nanocrystal film (red line) and oleylamine (black line).

REFERENCES

1 F. M. Courtel, R. W. Paynter, B. t. Marsan and M. Morin, *Chem. Mat.*, 2009, **21**, 3752-3762.

2 D. Pan, X. Wang, Z. H. Zhou, W. Chen, C. Xu and Y. Lu, *Chem. Mat.*, 2009, **21**, 2489-2493.

3 In *Handbook of x-ray photoelectron spectroscopy,* ed. J. F. Moulder, W. F. Stickle, P. E. Sobol and K. D. Bomben, Physical Electronics, 1992.

4 M.-Y. Chiang, S.-H. Chang, C.-Y. Chen, F.-W. Yuan and H.-Y. Tuan, *The Journal of Physical Chemistry C*, 2011, **115**, 1592-1599.

5 B. Canava, J. Vigneron, A. Etcheberry, D. Guimard, P. P. Grand, J. F. Guillemoles, D. Lincot, S. Ould Saad Hamatly, Z. Djebbour and D. Mencaraglia, *Thin Solid Films*, 2003, **431-432**, 289-295.

6 D. K. Suri, K. C. Nagpal and G. K. Chadha, *J. Appl. Crystallogr.*, 1989, **22**, 578-583.

7 M. Souilah, A. Lafond, N. Barreau, C. Guillot-Deudon and J. Kessler, *Appl. Phys. Lett.*, 2008, **92**, 241923.

8 M. Souilah, X. Rocquefelte, A. Lafond, C. Guillot-Deudon, J. P. Morniroli and J. Kessler, *Thin Solid Films*, 2009, **517**, 2145-2148.

9 S. T. Tan, B. J. Chen, X. W. Sun, W. J. Fan, H. S. Kwok, X. H. Zhang and S. J. Chua, *J. Appl. Phys.*, 2005, **98**, 013505.

10 R. Noufi, R. Powell, C. Herrington and T. Coutts, *Solar Cells*, 1986, **17**, 303-307.

11 S. H. Wei and A. Zunger, *J. Appl. Phys.*, 1995, **78**, 3846-3856.

12 (a) In *Handbook of photovoltaic science and engineering*,ed. A. Luque, S. Hegedus, Wiley, 2003; (b) F. Kang, J. P. Ao, G. Z. Sun, Q. He and Y. Sun, *Semicond. Sci. Technol.*, 2009, **24**,075015.

13 H. Zhong, S. S. Lo, T. Mirkovic, Y. Li, Y. Ding, Y. Li and G. D. Scholes, *ACS Nano*, 2010, **4**,

5253-5262.

14 E. Kucur, J. Riegler, G. A. Urban and T. Nann, *J. Chem. Phys.*, 2003, **119**, 2333-2337.